

In vivo performance analysis of silanized and coated nitinol wires in biological environment

Sarmita Sinha¹, Jyotsana Priyadarshani², Karuppasamy Bavya Devi^{3,c)}, Anyam Vijay Kishore⁴, Piyali Das⁴, Abhijit Chanda^{1,a)}, Soumen Das², Mangal Roy³, Samit Kumar Nandi^{4,b)}

¹Department of Mechanical Engineering, Jadavpur University, Kolkata 700032, India

²School of Medical Science and Technology, Indian Institute of Technology-Kharagpur, Kharagpur 721302, India

³Department of Metallurgical and Materials Engineering, Indian Institute of Technology-Kharagpur, Kharagpur 721302, India

⁴Department of Veterinary Surgery and Radiology, West Bengal University of Animal and Fishery Sciences, Kolkata 700037, India

^{a)}Address all correspondence to these authors. e-mail: abhijitchanda.biomed@gmail.com

^{b)}e-mail: samitnandi1967@gmail.com

^{c)}Present address: Department of Chemistry, Nims Institute of Engineering & Technology, Nims University Rajasthan, Jaipur-Delhi Highway (NH-11C), Nims Institute of Engineering & Technology, Jaipur-303121, Rajasthan, India.

Received: 13 February 2020; accepted: 8 April 2020

Some interesting properties such as superelasticity, shape memory effect, kink resistance, good biocompatibility, biomechanical properties, and corrosion resistance made nitinol a popular biomaterial as stent and orthopedic implants. But surface modification is needed to control nickel leaching from its surface, making safe for human body. The aim of this study was to modify the nitinol surface by the silanization technique and electrophoretically deposited hydroxyapatite coating, and to conduct a detailed in vitro and in vivo investigation. Detailed in vitro investigation involved MTT assay with the human osteoblastic cells (MG63 cell) over a period of 5 days and confocal image study. In case of in vivo study, histological study, fluorochrome labeling study, and Micro-Ct study were conducted. The overall in vitro and in vivo results indicate that silanized nitinol samples are showing slightly better level of performance, but both the surface-modified samples are suitable as the potential bio-implant for orthopedic purpose.

Introduction

Nitinol is a nickel–titanium metallic alloy with equiatomic composition which has exceptional physical and mechanical properties, shape memory effect, super-elastic properties, low elastic modulus, high strength, good corrosion resistance, and excellent biocompatibility [1, 2, 3]. These properties together with the similar biomechanical properties of human bone tissue make nitinol a promising biomaterial for orthopedic implant applications [4, 5]. But there are certain limitations as well. The corrosion property as well as discharge of nickel ions of NiTi shape memory alloys (SMA) has restricted its use in human organisms [6]. Chemical and thermal treatments may cause to abolish or diminish the surface Ni content of the alloy vis-à-vis accelerate to form a biocompatible titanium oxide on the surface of the alloy [7]. But this oxide layer is reported to show poor bioactivity. Moreover, it does not promote ready bonding with living tissues such as bone [8]. The surface coating with calcium phosphate-based compounds such as

hydroxide (inherently bioactive in nature) can ensure good corrosion resistance activity in addition to cell growth on it [9, 10, 11]. Various methods are in vogue to deposit calcium phosphate-based coatings such as plasma spray, electrophoretic deposition, sol–gel, biomimetic method, ion beam deposition, and electrochemical deposition [10, 12, 13, 14, 15, 16]. Numerous studies are there on in vitro cell culture on bare and surface-treated nitinol, but almost no reports are available on their detailed animal trial [17, 18, 19]. Another approach of surface modification in the form of bio-functionalization on nitinol is also being tried and is reported to give mixed results so far [20, 21]. Bio-functionalization is an easy surface modification process which involves permanent or temporary alteration with a biologically compatible material to have specific biological function. Various types of medical implants, tissue engineering-based scaffolds, cell culture platforms, drug delivery systems, and imaging probes are frequently bio-functionalized. In general, proteins and peptides in coupling

with biomaterials modify cell phenotype or tissue response. In 2016, Zhao et al. have done gelatin-functionalized graphene oxide coating on nitinol and found better antimicrobial activity and improved biocompatibility on nitinol [22]. Simsekylmaz et al. coated nitinol stents with star PEG, bio-functionalized with Arginine-Glycine-Aspartic (RGD) or RGD/CXCL1, and implanted into the carotid arteries of mice with considerably minimum neointima and thrombus formation [23]. In 2017, Karaji and his team have developed multifunctional porous super-elastic nitinol by additive manufacturing (selective laser melting) with a sensibly designed micro-architecture and bio-functionalized the surface using polydopamine-immobilized rhBMP2 for better control of the release kinetics [24]. They found enhanced cell attachment, cell proliferation, cell morphology, cell coverage, increased ALP activity, and calcium content on bio-functionalized surfaces as compared with as-manufactured specimens. In 2018, we have reported that the in vivo performance of silanized nitinol even without subsequent bio-functionalization with biopolymers was comparatively better than that of bare nitinol [25]. This betterment was observed in terms of various parameters and was attributed to the presence of Si, known to stimulate osseous ingrowth.

A critical overview of the available literature clearly suggests that till date a number of publications on surface modification of nitinol are there, but no comprehensive and systematic report on both in vitro and in vivo comparative performance of functionalized and coated nitinol is available. The present study presents a detailed report on both in vitro cell culture and in vivo animal trial of surface-modified nitinol, both silanized and HAp coated.

Results and discussion

The X-Ray Diffraction (XRD) patterns of pure HAp and HAp powder scratched from coated NiTi are shown in Figs. 1(A) and 1(B). Most peaks in both the samples were identified as HAp (JCPDS No. 09-0432). Minor amount of secondary phase of α -tricalcium phosphate (JCPDS No. 09-0348) was also found. Surface morphology of bare, silanized, and HAp-coated NiTi is shown in Fig. 1(C); Energy-dispersive X-ray spectroscopy (EDS) spectrum confirms the presence of Ni and Ti. Field Emission Scanning Electron Microscope (FESEM) of bare nitinol showed parallel striations which may be attributed to the mechanical polishing, whereas the FESEM of silanized nitinol did not show any major change in the basic texture; however, the application of (3-Aminopropyl)triethoxysilane (APTES) added some new features in the form of patches or droplets on the surface of the sample. The EDS spectrum of silanized NiTi did not show any peak of Si because of small percentage of APTES. However, we have confirmed the evidence of silanization using X-ray photoelectron spectroscopy (XPS) in our previous studies [25]. The HAp-coated NiTi

showed layer-by-layer deposition of globular shaped nonuniform coating. The presence of Ca and P on the coating was confirmed by EDS. Coating showed reasonably good adherence.

MTT assay [Fig. 2(a)] showed that at day 1, osteoblasts exhibited higher degree of proliferation on coated HAp samples than on silanized and bare NiTi. This increase in proliferation may be due to higher surface roughness of HAp-coated sample which was found to be 0.56 μm compared with silanized (0.142 μm) and bare (0.09) sample. At day 5, compared with bare NiTi, silanized NiTi showed better proliferation followed by coated NiTi samples. This betterment is because of the presence of Si. To promote osseous bone growth of Si, a well-known element played a crucial role in cell-material interaction [26]. The 2D and 3D confocal images after 5 days culture are shown in Fig. 2(b). It was observed that in case of HAp-coated NiTi, osteoblast cell growth seemed to be higher followed by silanized and bare NiTi samples. In all the cases, nucleus was clearly observed throughout the surface, which indicated normal growth of the cells and as such no sign of strain was observed on the cells. Thus, it reveals good cell viability on all the NiTi samples.

Radiography imaging helps to appreciate the time-dependent degradation vis-a-vis the bone formation, and the images are shown in Fig. 3(a). The skiagram of control after one month showed that the defect was observed to be obliterated partially with new osseous tissue. The cortical line was faintly visible and discontinuous. After three months, the gap was completely filled up with neo-osteogenic tissue with cortical continuation. At this stage, the medullary cavity at the defect site was observed to be more radiolucent and incomplete remodeling was observed. The radiograph of bare NiTi showed the evidence of implant occupying the defect without any perceptible change of radiodensity. Subsequently, on three months, the skiagram evidenced compactly anchored implant at the defect site, and the cortical line had been tightly adhered with the exterior age of the implant, indicating the process of remodeling of the defect. In case of silanized NiTi implant at one month, there was periosteal reaction around the exterior extremities. At this time point, hyperdense newly formed osseous tissue was observed partially obliterating the defect along the line of implant. Subsequently, after three months, the skiagram showed complete continuity of the cortical line at the defect site and compactly adhered implant within the medullary cavity. The radiodensity of the implant appears to be unaltered, indicating the advance stage of remodeling. The radiograph of coated NiTi sample at one month showed compactly adhered implant at the defect with a well-defined thick cortical line adjacent to the defect; the implant seemed to be radiologically unaltered in term of size, shape, and density. Finally, at three months, complete obliteration of defect was noticed with continuous cortical line of similar radiological features to that of adjacent host site. The implant was noticed within the medullary cavity without alteration of density, size, and shape.

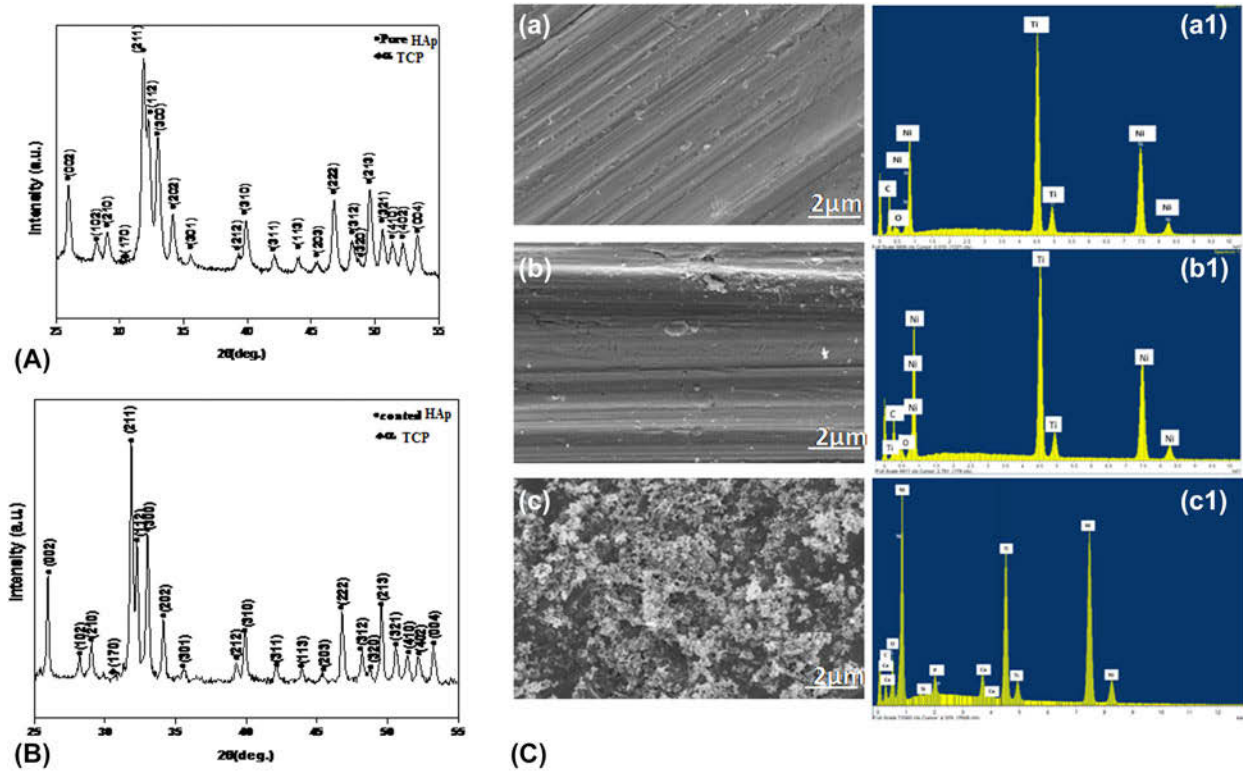


Figure 1: (A) XRD of pure HAp (B) scratched HAp from the coated NiTi (C) FESEM and Energy dispersive X-Ray (EDX) of (a, a1) bare NiTi, (b, b1) silanized NiTi, and (c, c1) Hap-coated NiTi.

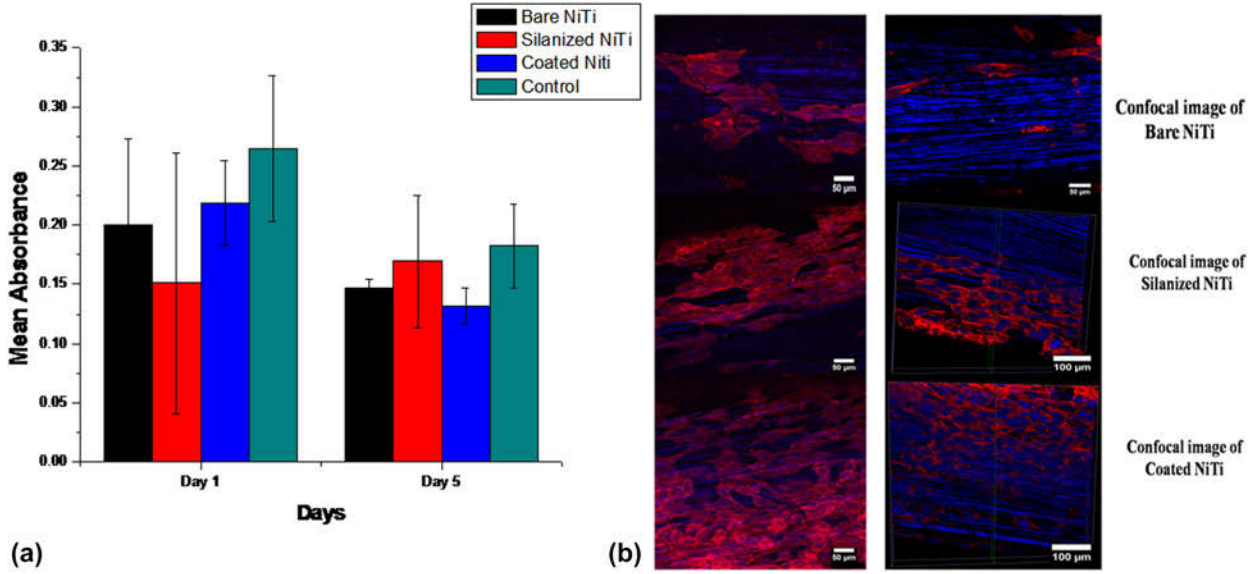


Figure 2: (a) MTT assay analysis of control, bare NiTi, silanized NiTi, and Hap-coated NiTi and (b) 2D and 3D confocal micrographs of bare NiTi, silanized NiTi, and coated NiTi samples.

The in vivo bone regeneration and the bone-material interaction of all the bone samples were analyzed using micro-computed tomography, and the 2D and 3D images are shown in Figs. 3(b) and 3(c). The 1M post-implanted 2D micro-CT images [Fig. 3(b)] of bare, silanized samples due to

the presence of Si and Hap-coated NiTi showed characteristic irregular new osseous tissue formation around the implant materials, whereas the control samples showed no onset of bony tissue formation. The postoperated 2D radiographs of silanized NiTi at three months showed complete closure of the

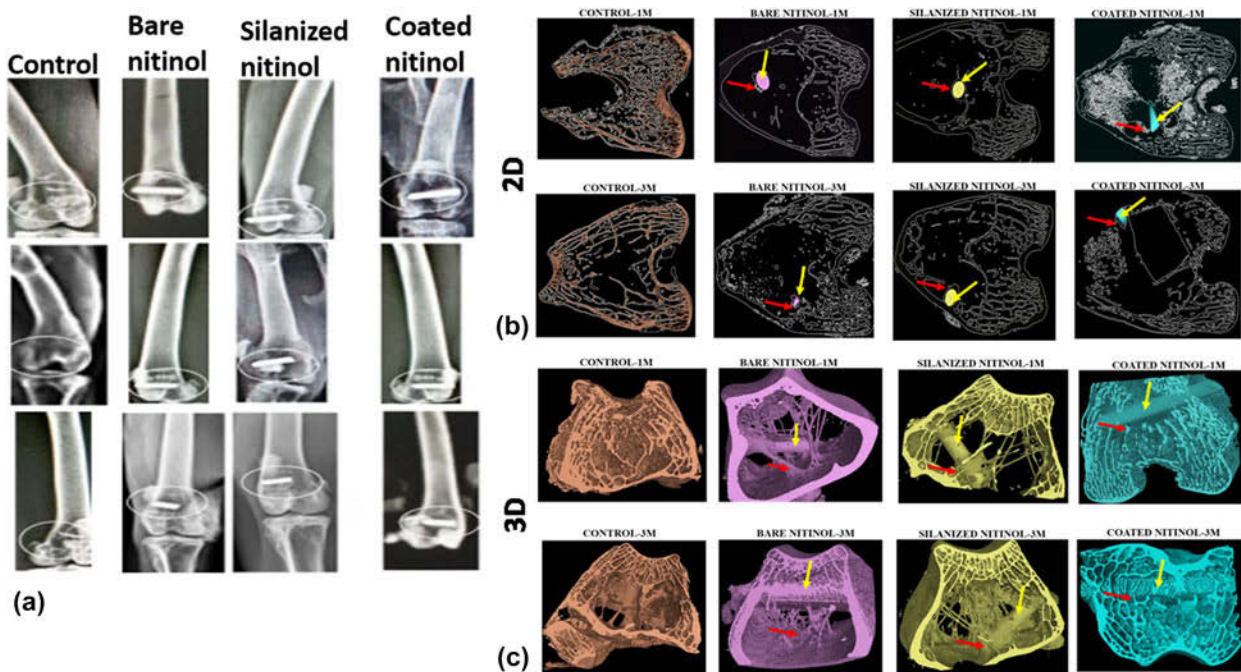


Figure 3: (a) Radiological images of control sample, bare NiTi, silanized NiTi, and coated NiTi sample on 0, 1, and 3 months, (b) radiographic 2D, and (c) 3D images of defect bone sites showing extent of healing after 1 and 3 months (red arrow showing new bone growth around the implant; yellow arrow showing implant material).

defect size and higher amount of bony tissue (shown by red arrow) fully covering the implant material followed by Hap-coated and bare NiTi. It may be credited to the release of Si ions compared with other samples that played a noteworthy role in enhancing the new bone formation. The one month 3D images [Fig. 3(c)] of bare, silanized, and Hap-coated NiTi showed that the implanted samples showed that bone has started to grow on all the implants, indicating the osteoconductive nature of the material. With the passage of time from 1 to 3 months, partial bone accumulation are seen inside and around the defect area for bare and Hap-coated NiTi, whereas silanized NiTi showed finer and matured bone formation completely filling the defect hole, showing the complete formation of periosteum. The resorption process was more distinct for silanized NiTi with thick newly formed bony tissue, and large struts of trabecular bone were formed on the implant. The enhanced bone growth for silanized NiTi may be as a result of the positive effect of silicon [26].

A comparative examination suggests that in silanized sample there was a closely knit bony tissue structure around the foreign material. It was so dense that the specimen could hardly be noticed. In case the periosteum was completely formed with uniform thickness, there was a clear sign of growing natural bone tissue. The presence of Si played an important role in enhancing the bone regeneration [27, 28]. The released Si ions got embedded inside the nearby bony tissue served as a stimulant for bone marrow stromal cell

differentiation and osteoblastic proliferation, which resulted in the complete formation of periosteum [29]. Similar studies of Kim et al. also showed that the released Si ions from Si-doped HAp resulted in enhanced bone growth and faster healing of defect site in the rabbit model [30]. Moreover, Si is important in elevating the synthesis of collagen type 1 and osteoblast differentiation, and it also helps in early bone repair at the defect site [31]. Figures 4(a)–4(d), 4(i)–4(l), and 4(q) show oxytetracycline labeling images of new bone formation. The photomicrograph of the fluorochrome studies of control group at one month depicted bright yellow fluorescence of newly formed bony tissue (28%) at the center of sea green backdrop. At the same time point, the bare nitinol group showed more formation of newly formed bony tissue (38%) as bright golden fluorescence as compared with the control one. The silanized (51%) and coated nitinol (53%) showed abundance of golden yellow fluorescence in more regions. At 3 months, the photomicrograph of control sample showed moderate golden yellow fluorescence of osseous tissue (33%) in a scattered zone. The golden yellow fluorescence of newly formed bony tissue (51%) was observed throughout the section of the bare nitinol. The silanized nitinol group (71%) showed a wide area of golden yellow fluorescence as compared with its earlier time point, indicating the active state of bone regeneration. Finally, the coated nitinol group (73%) showed more golden yellow fluorescence in a wide region in the background of deep green sea colored host tissue. Figures 4(e)–4(h) and 4(m)–4(p)

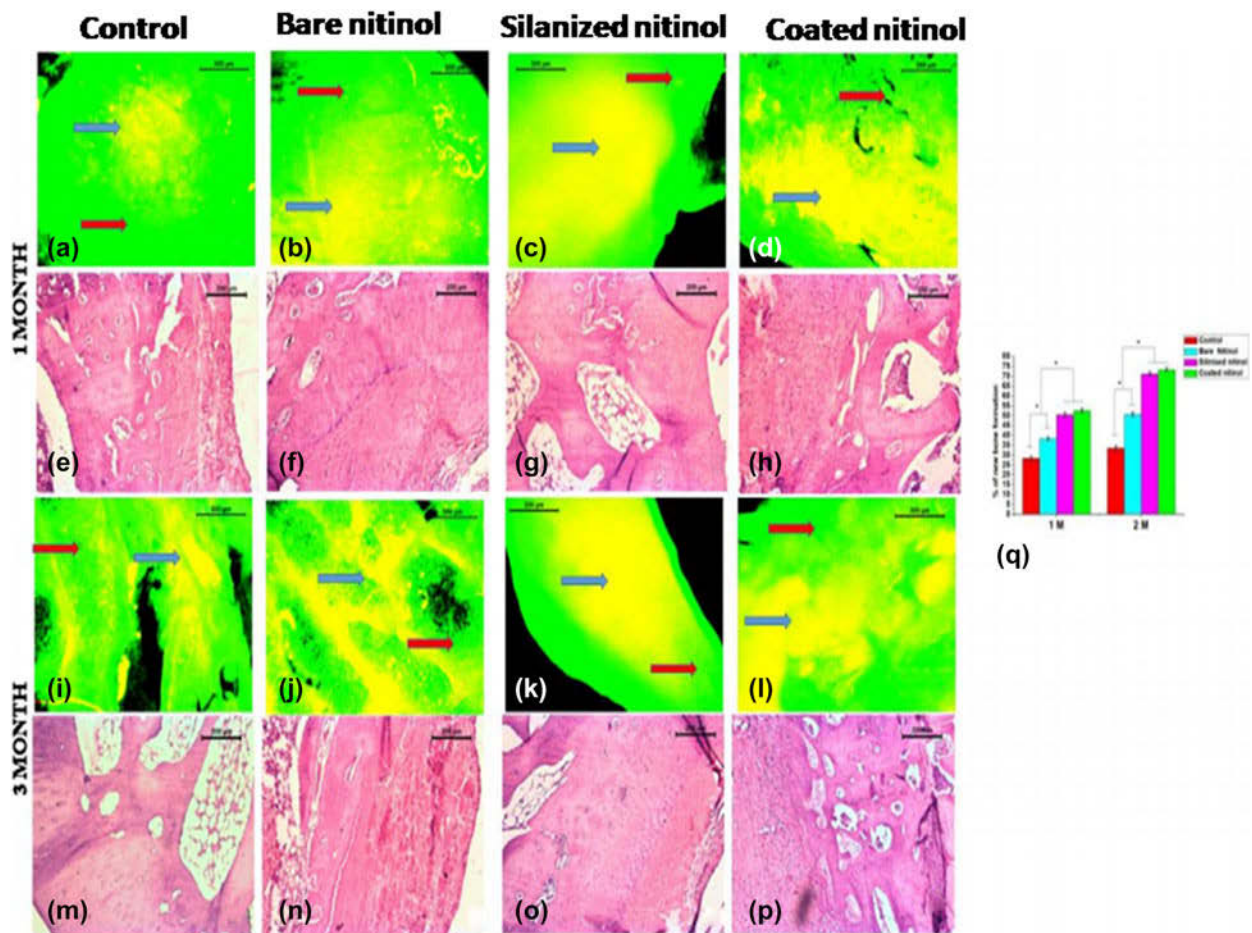


Figure 4: Fluorochrome labeling (a–d) (i–l) and histological images (e–h) (m–p) of control sample, bare NiTi, silanized NiTi, and coated NiTi sample after 1 and 3 months (blue arrow: new bone; red arrow: old bone). (q) Bar diagram of statistical presentation of new cell formation.

showed the histological images at 1- and 3-month time points of control and implanted samples. The section of the control sample after 1 month depicted bony tissues along with perichondrium arranged orderly along with the proliferation of few osteoblast and osteoclast. The osteocytes were well arranged with the presence of fat cells, few osteoblast, red blood cells (RBC), and scanty fibrinous deposit at medullary spaces. However, the section after 3 months showed a bony structure containing osteoblast and osteocytes. The Haversian canal was laid by fibrinous matrix and the presence of few osteocytes around the lacunar spaces. The pericortical spaces contained fibrocartilagenous structure invaded by few osteocytes. The photomicrograph of the sample containing bare nitinol after 1 month showed bony tissue with osteoclastic activity around the peri-medullary spaces. The medullary cavity had abundant osteoblast, RBC, and fibrinous exudate. In case of 3 months, the bony structure consists of abundant Haversian canal, sinusoidal space, and few lacunae. The entire osteogenic stroma was embedded with abundant osteoclast, osteoblast in definite arranged manner. The silanized sample at 3 months showed

solid osteogenic proliferation with the presence of abundant osteoblast and osteoclast. The Haversian canal was well arranged, and the lacunar spaces contained few osteocytes and fat cells. The medullary cavity contained scanty RBC and fibrinous deposit. Finally, the Hap-coated nitinol sample at 1 month depicted a newly formed bony osteoid containing multiple osteoblast and osteoclast. The pericortical spaces were rich in osteocytic cell, fibrinous exudate, and abundant RBC. The lining area of medullary spaces was enriched with multiple osteocytes and Haversian canal. In comparison with 1 month, the coated nitinol sample at 3 months showed well-regenerated osteogenic stroma consisting of abundant osteoblast and osteoclast. The total osteoid was invaded by abundant vascular channels. The medullary cavity contained osteocytes, RBC, and mild fibrinous deposit.

Conclusion

This study provided a thorough insight in silanization of bare NiTi surface using APTES and also involved electrophoretic

deposition of pure HAp on bare NiTi surface, where HAp was synthesized by wet chemical process. The coating process by electrophoretic deposition was thoroughly optimized. Fluoro-chrome labeling study and confocal images showed better performance in case of coated NiTi sample; but based on the cell proliferation, histological, radiological, and micro-CT study, the silanized NiTi implant showed better performance and confirmation of faster bone formation. From 3D micro-CT images, finer and matured bone formation completely filling the defect hole and showing the complete formation of periosteum was shown. Silanization increased the early stage in vivo implant-bone assimilation and bone remodeling. The detailed and overall in vivo and in vitro characteristics of silanized and coated Nitinol reveal that in most studies, silanized samples performed better than the coated one. However, the main importance of the study is that it opens a new vista for better fixation of implant at the fracture site.

Materials and methods

Materials

The material for these experiments was commercially available nitinol shape memory wire. 1.5 mm diameter nitinol alloy wire consists of 54.5 wt% Ni and 45.5 wt% Ti (Manufacturer: Nitinol Devices & Components, NDC, California; Supplier: VRAS traders, India). As per the specification of the supplier, the composition conforms well to ASTM F-2063. The basic chemicals used were Acetone (Merck, Mumbai, India), Ethanol (Merck), ortho-phosphoric acid (Merck), and calcium hydroxide (Merck).

Human osteoblast cells (MG 63) were obtained from the National Centre for Cell Science (NCCS), Pune, India, and the cells were preserved following the standard protocol.

Methods

The NiTi wire of 1.5 mm diameter was cut into a number of pieces with length 1 cm each followed by washing thoroughly for 15 min with acetone (70% by volume), ethanol, and deionized water, respectively. These washing processes were done to get rid of residual surface impurities, and then finally dried to use for coating and other various studies. Before sterilization/washing processes, the samples which were used for coating were polished with 220 SiC paper.

The methodology of the silanization process was described in our previous study [25]. Calcium hydroxyapatite (HAp) powder was prepared by following the standard wet chemical method, using A.R. grade calcium hydroxide $[\text{Ca}(\text{OH})_2]$ and ortho-phosphoric acid $[\text{H}_3\text{PO}_4]$. During the reaction, the pH was maintained at 11–12 at 80 °C. The solution accordingly obtained was placed for 24 h, followed by filtration. The precipitate was allowed to dry at 80 °C for 24 h and then

subsequently calcined at 800 °C for 2 h, to obtain the optimum crystallinity. This HAp powder was used in electrophoretic deposition in a simple laboratory setup. To prevent the gas formation due to the hydrolysis of water, 99% ethanol was used as a solvent during electrophoresis resulting in the deposition of uniform adherent hydroxyapatite coating [1, 2]. The colloidal suspension was placed in a magnetic stirrer for 60 min and after that in an ultrasonic bath for 60 min. Hydroxyapatite from the colloidal suspension was deposited on NiTi samples using the electrophoretic deposition (EPD) technique. The NiTi substrate was used as a cathode and as a counter electrode also. The electrodes were placed parallel to each other within a distance of 15 mm and connected to the power supply enabling current measurements. The standardized voltage for this work was 60 V and deposition time of 10–90 min were applied. All EPD experiments were carried out at ambient temperature. After deposition, the green coatings were dried at 80 °C for 2 h.

Using Rigaku diffractometer, Ultima-III, Rigaku Co., Tokyo, Japan, X-ray diffraction analysis was performed on the deposited powder to check if there was any change in the form of hydroxyapatite after electrophoresis. FESEM study was carried out using the JEOL JSM-5200 model, Tokyo, Japan, and EDX study was carried out with JEOL JSM-6360 Tokyo, Japan. Finally, surface roughness was measured with Talysurf Plus Sardonis, 3P, England.

In vitro study

An in vitro cell culture was carried out using MG63 osteoblastic cell line. A quantitative colorimetric measurement of extracellular reduction of the yellow-colored Tetrazolium dye 3-[4,5-dimethylthiazol-2-yl]-2,5-diphenyl tetrazolium bromide (MTT, HiMedia, India) to insoluble purple formazan crystals was performed to analyze cell viability percentage. MTT assay was prepared in phosphate buffer solution (PBS) at a concentration of 4.2 mg/mL, and 100 μL of this solution was mixed with 400 μL of cell culture media and poured in each well of the 48-well plate with the cells. Furthermore, well plate was incubated inside 5% CO_2 incubator at 37 °C for 4 h. Afterward, media was discarded and residual water-insoluble formazan crystals were dissolved in 200 μL of dimethylsiloxane (DMSO) in each well. After vigorously mixing the crystals in DMSO, a purple solution is formed which was transferred into a 96-well plate for colorimetric reading in spectrophotometer plate reader (Multiskan GO, Thermo Fisher Scientific, India). Detailed MTT assay analysis was performed with bare nitinol, silanized nitinol, and Hap-coated nitinol samples for a span of 5 days, where data were taken on intermittently on 1st and 5th day.

Cell proliferation study of osteoblast cells were conducted using confocal microscopic technique. The confocal laser

pictographs were obtained after 5 days of culture period. To fix the cells, all the samples were fixed with 4% paraformaldehyde at room temperature for 20 min and washed with 1× PBS three times. Next, samples were permeabilized with 0.1% Triton X-100 for 10 min and again washed with PBS thrice. Blocking agent 1% BSA was added to each samples to reduce background noise for 1 h followed by rhodamine-phalloidin (Invitrogen™, Thermo fisher Scientific) staining with time duration of 45 min, which were washed properly with PBS. For nucleus staining, 4',6-diamidino-2-phenylindole (DAPI) was used for 5–10 min and again washed with PBS. All the samples were stored in PBS at 4 °C until imaging. Images were taken using a confocal laser scanning microscope (Leica, TCS, SP8). The 3D multichannel image processing was performed using Leica Application Suite X (LAS X).

In Vivo study

Animal experimentation was performed as per the standard procedures of the Institutions' Animal Ethical Committee of the West Bengal University of Animal and Fishery Sciences, Kolkata, India [Permit No. Pharma/188(ix) dated 31.07.2015]. Healthy New Zealand white rabbits of both gender, weighing 2–2.5 kg were randomly divided into four groups: control group I (without any implant), group II (bare nitinol implants were inserted within the created bone defects), group III (silanized nitinol were inserted within the created bone defects), and group IV (Hap-coated nitinol implants were inserted within the bone defects) [Table I]. Figure 5 showed the well-placed nitinol implant in rabbit distal epiphysis of femur. The specimen was implanted transversely within the created defects in the distal metaphysis of femur. Before surgery, the rabbits were kept individually in separate cages with alternating 12 h cycles of light and dark in temperature- and humidity-controlled rooms, given water ad libitum, and were without restriction of movement. Anesthesia was achieved injecting a dose of 1 mg/kg body weight of Xylazine hydrochloride (XYLAXIN®, Indian Immunologicals, India) and Ketamine hydrochloride (Ketalar®, Parke-Davis, India) at a dose of 25 mg/kg body weight intramuscularly. A bone defect (5 × 1.5 mm) in each animal was created in the medial aspect of distal epiphysis of femur bone with the help of a motorized dental drill. The implant was inserted in press-fit manner within the created bone defects and secured in position by suturing muscle, subcutaneous tissue, and skin in layers.

Local inflammatory reaction and healing of wound

All the animals were closely observed for lameness, weight-bearing capacity, and swelling of the surgical area, and related signs of local inflammatory reactions were observed from

TABLE I: Animal group type.

Group I	Control group
Group II	Test animals with bare nitinol implant
Group III	Test animals with silanized nitinol implant
Group IV	Test animals with electrophoretically Hap-coated nitinol implant

the day of operation postoperatively and changes were evaluated by visual and manual examinations. All the treated animals were administered using injection, cefotaxim sodium (Mapra India, India) at a dose rate 65 mg per animal intramuscularly, at 12 h interval daily for 5 days, and meloxicam (Melonex®, Intas Pharmaceuticals, India) at 0.1 mL once daily for 5 days were given. Dressing of surgical wounds was carried out using povidone iodine lotion and antibiotic ointment for 10 days postoperatively. Radiographs were taken just after operation, on 30th and 90th day post-operatively of the operated distal epiphysis femur bone for studying the position of implant and host bone reaction to implant.

Histology

The nitinol-implanted distal femoral epiphysis was collected at the day of sacrifice for histological analysis to check the cellular response bone to the implants. The implanted nitinol implants along with the surrounding bones were collected from the animals after sacrificing the animal. The bone pieces (3–4 mm thick) were taken from implanted area and were cut (3–4 mm thick) using a hacksaw. These bone specimens from adjacent bone at the side and at the bottom of the original bone defect were collected and washed thoroughly with normal saline and were fixed in 10% formalin for 7 days. All specimens of bone tissue were decalcified using Goodling and Stewart's fluid (formic acid 15 mL, formalin 5 mL, and distilled water 80 mL solution), followed by fixation with 4% paraformaldehyde. Finally, the decalcified bone tissues were embedded into paraffin wax for preparation of 4 µm thick sections and stained with hematoxylin and eosin.

Micro-computed tomography

To study the nature of the implant, host bone-implant interactions and the new bone formation, the postoperated bone samples were analyzed using micro-CT (Phoenix V|tome|xS, GE, Germany). All the bone samples were completely dried at room temperature. The bone samples were scanned at a voltage of 85 kV and a current of 70 µA, with a voxel size of 18 µm. Time fraction was 500 ms per image with 1000 images in one complete rotation. The constructed 2D images were compiled to build 3D models using VG studio MAX 2.2 software (Volume Graphics, Germany).

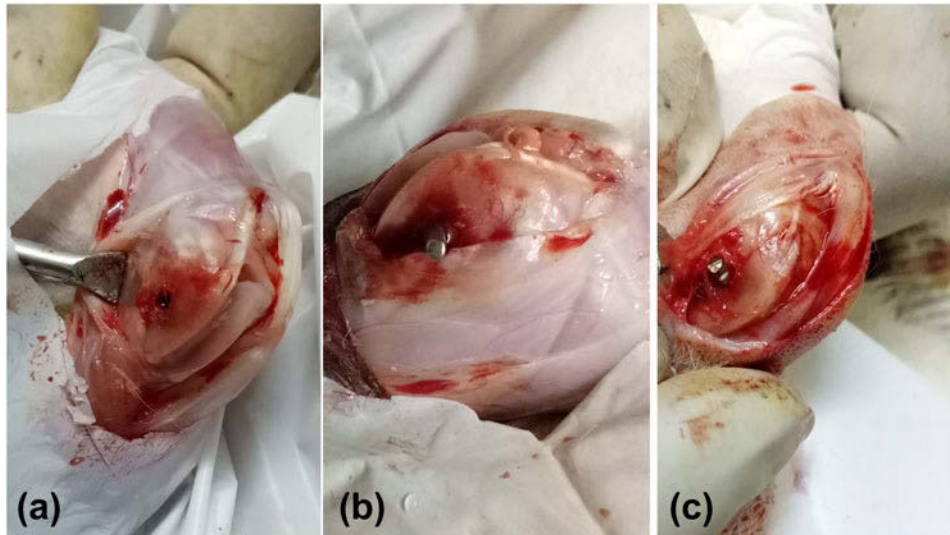


Figure 5: (a) Bone defect, (b) coated nitinol in the bone defect, and (c) silanized nitinol in bone defect.

Radiology

Radiographs were taken just after operation, 1 and 3 months postoperatively of the operated distal epiphysis femur bone for studying the position of implant and host bone reaction to implant.

Oxytetracycline labeling study

Fluorochrome (oxytetracycline dehydrate; Pfizer India, India) was injected at 25 mg/kg body weight, 25 days before euthanizing the animal at 1 month time point, that is, on the days 5, 6, and 13, and 14, and for 3 months sample, on days 65, 66, and 73, and 74 (2-6-2 manner) for double toning of new bone. The implanted bone segments were retrieved at the aforementioned time points and undecalcified, polished 15–20 μm thickness bone specimens were prepared. During preparation, the bone samples were kept dipping from time to time in water during the entire procedure. The polished thin bone sections were observed under UV light with Leica DM 2000 Bright light phase contrast and fluorescence microscope, including Leica Qwain software. Oxytetracycline marker shows golden yellow fluorescence (new bone formation) and sea green hue (host bone). The golden yellow and sea green color pixels areas have been measured from the figure and average values were taken and statistically analyzed.

Statistical analysis

Statistical analysis of the fluorochrome labeling data was carried out using one-way analysis of variance (ANOVA) with a Tukey's post hoc by ORIGIN software. Absolute mean values and standard deviations (SDs) were calculated. Data were taken from three samples ($n = 3$).

Acknowledgments

One of the authors Sarmita Sinha would like to acknowledge the Council of Scientific and Industrial Research. The authors wish to express their thanks to the Honorable Vice-Chancellor of West Bengal University of Animal and Fishery Sciences, Kolkata, India. Authors also acknowledge Mechanical Engineering Department and School of Bio Science & Engineering, Jadavpur University, Kolkata, India, for their support to use the facilities for the experimentation. Mangal Roy would like to acknowledge technical personnel at the Central Facility, IIT-Kharagpur, for their support in μ -CT analysis.

References

1. C.H. Fu, P.M. Sealy, Y.B. Guo, and X.T. Wei: Austenite–martensite phase transformation of biomedical nitinol by ball burnishing. *J. Mater. Process. Technol.* **214**, 3122 (2014).
2. F.L. Nie, Y.F. Zheng, Y. Cheng, S.C. Wei, and R.Z. Valiev: In vitro corrosion and cytotoxicity on microcrystalline, nanocrystalline, and amorphous NiTi alloy fabricated by high pressure torsion. *Mater. Lett.* **64**, 983 (2010).
3. I. Gotman, D. Ben-David, R.E. Unger, T. Böse, E.Y. Gutmanas, and C.J. Kirkpatrick: Mesenchymal stem cell proliferation and differentiation on load-bearing trabecular nitinol scaffolds. *Acta Biomater.* **9**, 8440 (2013).
4. M. Akmal, A. Raza, M.M. Khan, M.I. Khan, and M.A. Hussain: Effect of nano-hydroxyapatite reinforcement in mechanically alloyed NiTi composites for biomedical implant. *Mater. Sci. Eng., C* **68**, 30 (2016).
5. S. Kamali, S. Shemshad, A. Khavandi, and S. Azari: Construction novel hydroxyapatite-nitinol nanocomposite for hard tissue applications. *Mater. Chem. Phys.* **220**, 331 (2018).

6. **J. Khalil-Allafi, B. Amin-Ahmadi, and M. Zare:** Biocompatibility and corrosion behavior of the shape memory NiTi alloy in the physiological environments simulated with body fluids for medical applications. *Mater. Sci. Eng., C* **30**, 1112 (2010).
7. **S.A. Shabalovskaya, H. Tian, J.W. Andereg, D.U. Schryvers, W.U. Carroll, and J.V. Humbeeck:** The influence of surface oxides on the distribution and release of nickel from nitinol wires. *Biomaterials* **30**, 468 (2009).
8. **S.A. Shabalovskaya, J. Andereg, F. Laab, P.A. Thiel, and G. Rondelli:** Surface conditions of nitinol wires, tubing, and as-cast alloys. The effect of chemical etching, aging in boiling water, and heat treatment. *J. Biomed. Mater. Res., Part B* **65**, 193 (2003).
9. **R. Singh and N.B. Dahotre:** Corrosion degradation and prevention by surface modification of biometallic materials. *J. Mater. Sci.: Mater. Med.* **18**, 725 (2007).
10. **F. Sun, X. Pang, and I. Zhitomirsky:** Electrophoretic deposition of composite hydroxyapatite–chitosan–heparin coatings. *J. Mater. Process. Technol.* **209**, 1597 (2009).
11. **K. Dudek, M. Plawewski, M. Dulski, and J. Kubacki:** Multifunctional layers formation on the surface of NiTi SMA during β -tricalcium phosphate deposition. *Mater. Lett.* **157**, 295 (2015).
12. **Y.C. Tsui, C. Doyle, and T.W. Clyne:** Plasma sprayed hydroxyapatite coatings on titanium substrates. Part 2: Optimisation of coating properties. *Biomaterials* **19**, 2031 (1998).
13. **M.F. Hsieh, L.H. Perng, T.S. Chin, and H.G. Perng:** Phase purity of sol–gel-derived hydroxyapatite ceramic. *Biomaterials* **22**, 2601 (2001).
14. **J. Venugopal, M.P. Prabhakaran, Y. Zhang, S. Low, A.T. Choon, and S. Ramakrishna:** Biomimetic hydroxyapatite-containing composite nanofibrous substrates for bone tissue engineering. *Philos. Trans. R. Soc., A* **368**, 2065 (2010).
15. **F.Z. Cui, Z.S. Luo, and Q.L. Feng:** Highly adhesive hydroxyapatite coatings on titanium alloy formed by ion beam assisted deposition. *J. Mater. Sci.: Mater. Med.* **8**, 403 (1997).
16. **M.R. Etminanfar and J. Khalil-Allafi:** On the electrodeposition of Ca–P coatings on nitinol alloy: A comparison between different surface modification methods. *J. Mater. Eng. Perform.* **25**, 466 (2016).
17. **M. Es-Souni, M. Es-Souni, and H. Fischer-Brandies:** On the properties of two binary NiTi shape memory alloys. Effects of surface finish on the corrosion behaviour and in vitro biocompatibility. *Biomaterials* **23**, 2887 (2002).
18. **Y. Li, T. Zhao, S. Wei, Y. Xiang, and H. Chen:** Effect of Ta₂O₅/TiO₂ thin film on mechanical properties, corrosion, and cell behavior of the NiTi alloy implanted with tantalum. *Mater. Sci. Eng., C* **30**, 1227 (2010).
19. **S.A. Bernard, V.K. Balla, N.M. Davies, S. Bose, and A. Bandyopadhyay:** Bone cell–materials interactions and Ni ion release of anodized equiatomic NiTi alloy. *Acta Biomater.* **7**, 1902 (2011).
20. **H.Y. Yeh and J.C. Lin:** Bioactivity and platelet adhesion study of a human thrombomodulin-immobilized nitinol surface. *J. Biomater. Sci. Polym. Ed.* **20**, 807 (2009).
21. **H. Yu, J. Yan, H. Ma, X. Zeng, Y. Liu, and X. Zhao:** Creating poly(ethylene glycol) film on the surface of NiTi alloy by gamma irradiation. *Radiat. Phys. Chem.* **112**, 199 (2015).
22. **C. Zhao, S. Pandit, Y. Fu, I. Mijakovic, A. Jesorka, and J. Liu:** Graphene oxide based coatings on nitinol for biomedical implant applications: Effectively promote mammalian cell growth but kill bacteria. *RSC Adv.* **6**, 38124 (2016).
23. **S. Simsekiylmaz, E.A. Liehn, S. Weinandy, F. Schreiber, R.T.A. Megens, W. Theelen, R. Smeets, S. Jockenhövel, T. Gries, M. Möller, D. Klee, C. Weber, and A. Zenecke:** Targeting instant-stenosis with RGD- and CXCL1-coated mini-stents in mice. *PLoS One* **11**, 155829 (2016).
24. **Z. Gorgin Karaji, M. Speir, S. Dadbakhsh, J.P. Kruth, H. Weinans, A.A. Zadpoor, and S.A. Yavari:** Additively manufactured and surface biofunctionalized porous nitinol. *ACS Appl. Mater. Interfaces* **9**, 1293 (2017).
25. **S. Sinha, H. Begam, V. Kumar, S.K. Nandi, J. Kubacki, and A. Chanda:** Improved performance of the functionalized nitinol as a prospective bone implant material. *J. Mater. Res.* **33**, 2554 (2018).
26. **L.F. Rodella, V. Bonazza, M. Labanca, C. Lonati, and R.A. Rezzani:** Review of the effects of dietary silicon intake on bone homeostasis and regeneration. *J. Nutr. Health Aging* **18**, 820 (2014).
27. **B.K. Devi, B. Tripathy, A. Roy, B. Lee, P.N. Kumta, S.K. Nandi, and M. Roy:** In vitro biodegradation and in vivo biocompatibility of forsterite bio-ceramics: Effects of strontium substitution. *ACS Biomater. Sci. Eng.* **5**, 530 (2019).
28. **K.A. Hing, P.A. Revell, N. Smith, and T. Buckland:** Effect of silicon level on rate, quality, and progression of bone healing within silicate-substituted porous hydroxyapatite scaffolds. *Biomaterials* **27**, 5014 (2006).
29. **M. Shi, Y. Zhou, J. Shao, Z. Chen, B. Song, J. Chang, C. Wu, and Y. Xiao:** Stimulation of osteogenesis and angiogenesis of HBMSCs by delivering Si ions and functional drug from mesoporous silica nanospheres. *Acta Biomater.* **21**, 178 (2015).
30. **B.S. Kim, S.S. Yang, J.H. Yoon, and J. Lee:** Enhanced bone regeneration by silicon-substituted hydroxyapatite derived from cuttlefish bone. *Clin. Oral Implants Res.* **28**, 49 (2017).
31. **C.T. Price, K.J. Koval, and J.R. Langford:** Silicon: A review of its potential role in the prevention and treatment of postmenopausal osteoporosis. *Int. J. Endocrinol.* **2013**, 316783 (2013).